Journal of Structural Biology xxx (xxxx) xxx–xxx

Contents lists available at ScienceDirect

Journal of Structural Biology

journal homepage: www.elsevier.com/locate/yjsbi

3D Fiber Orientation in Atherosclerotic Carotid Plaques

Ali C. Akyildiz[a,*], Chen-Ket Chai[b], Cees W.J. Oomens[b], Aad van der Lugt[c], Frank P.T. Baaijens[b], Gustav J. Strijkers[b,d], Frank J.H. Gijsen[a]

[a] Department of Biomedical Engineering, Erasmus Medical Center, Rotterdam, The Netherlands
[b] Department of Biomedical Engineering, Eindhoven University of Technology, Eindhoven, The Netherlands
[c] Department of Radiology, Erasmus Medical Center, Rotterdam, The Netherlands
[d] Biomedical Engineering and Physics, Academic Medical Center, University of Amsterdam, Amsterdam, The Netherlands

ARTICLE INFO

Keywords:
Collagen architecture
Carotid artery
Atherosclerosis
3D fiber direction
Pathological vessel

ABSTRACT

Atherosclerotic plaque rupture is the primary trigger of fatal cardiovascular events. Fibrillar collagen in atherosclerotic plaques and their directionality are anticipated to play a crucial role in plaque rupture. This study aimed assessing 3D fiber orientations and architecture in atherosclerotic plaques for the first time.

Seven carotid plaques were imaged ex-vivo with a state-of-the-art Diffusion Tensor Imaging (DTI) technique, using a high magnetic field (9.4 Tesla) MRI scanner. A 3D spin-echo sequence with uni-polar diffusion sensitizing pulsed field gradients was utilized for DTI and fiber directions were assessed from diffusion tensor measurements. The distribution of the 3D fiber orientations in atherosclerotic plaques were quantified and the principal fiber orientations (circumferential, longitudinal or radial) were determined.

Overall, 52% of the fiber orientations in the carotid plaque specimens were closest to the circumferential direction, 34% to the longitudinal direction, and 14% to the radial direction. Statistically no significant difference was measured in the amount of the fiber orientations between the concentric and eccentric plaque sites. However, concentric plaque sites showed a distinct structural organization, where the principally longitudinally oriented fibers were closer to the luminal side and the principally circumferentially oriented fibers were located more abluminally. The acquired unique information on 3D plaque fiber direction will help understanding pathobiological mechanisms of atherosclerotic plaque progression and pave the road to more realistic biomechanical plaque modeling for rupture assessment.

1. Introduction

Atherosclerotic plaque rupture in carotid arteries is strongly associated with cerebrovascular events (Carr et al., 1996). However, there are no reliable means to assess the rupture risk of atherosclerotic plaques. Hence, in the current clinical practice carotid plaque rupture risk is not taken into account when planning preventive treatment strategies. Biomechanical plaque stress analyses have the potential for assessing plaque rupture risk (Cheng et al., 1993; Richardson et al., 1989; Teng et al., 2014). The mechanical stresses in atherosclerotic plaques can be determined with finite element (FE) modeling techniques (Akyildiz et al., 2015; Nieuwstadt et al., 2013). A critical factor to obtain accurate stress results from FE models is the correct representation of the mechanical behavior of the plaque components in the models (Akyildiz et al., 2011; Teng et al., 2015).

The macroscopic mechanical behavior of biological tissues is governed by their microstructural composition. It is well established that in healthy arteries, collagen fibers are one of the main load bearing microstructures and their organization is a significant determinant of the arterial anisotropic mechanical behavior (Fratzl, 2008; Holzapfel et al., 2002; Humphrey, 2002). The vascular collagen comprises up to 50% of the dry weight and exists in all three layers of the healthy vessel wall (Bartoš and Ledvina, 1979; Hosoda et al., 1984; Mayne, 1986). In the innermost, thin tunica intima, collagen fibers show dispersed orientation and form a network underlying the endothelial cells to provide a physical support base (Canham et al., 1989; Finlay et al., 1995). In the tunica media, the collagen fibers are organized in a helical structure around the artery circumference (Clark and Glagov, 1985; Shadwick, 1999; Walker-Caprioglio et al., 1991). In tunica adventitia, the dispersedly oriented fibers show a wavy pattern at low intraluminal pressure and straighten with increasing pressure to protect the tissue from a potential acute overstretching (Canham et al., 1989; Finlay et al., 1995). A comprehensive review of the collagen architecture and its mechanical role in healthy arteries can be found in (Chen and

* Corresponding author.
E-mail address: a.akyildiz@erasmusmc.nl (A.C. Akyildiz).

http://dx.doi.org/10.1016/j.jsb.2017.08.003
Received 24 February 2017; Received in revised form 18 July 2017; Accepted 20 August 2017

Kassab, 2016; Holzapfel, 2008).

Fibrillar collagen is also abundantly present in atherosclerotic plaques (Rekhter et al., 1993) and as such, its organization is highly likely to be a key determinant of the mechanical behavior of the plaque material (Chai et al., 2015). During atherogenesis smooth muscle cells (SMCs) transmigrate from the tunica media into the tunica intima, leading to intimal hyperplasia, and transform from the contractile to the synthetic phenotype (Barnes and Farndale, 1999). The synthetic SMCs are responsible for collagen synthesis in the atherosclerotic plaques (Newby and Zaltsman, 1999). The presence and types of collagen in atherosclerotic arteries have been studied widely (Murata et al., 1986; Nadkarni et al., 2007; Pickering et al., 1996; Reimann et al., 2016). However data on collagen orientation and architecture is relatively scarce and provides only 2D information as it is mainly obtained from histological examinations (Deguchi et al., 2005; Orekhov et al., 1987; Shekhonin et al., 1985). Hence, there is a strong need for qualitative and quantitative data on the 3D collagen architecture in atherosclerotic plaques.

Diffusion Tensor Imaging (DTI) is a non-invasive magnetic resonance imaging (MRI) technique, which is a powerful tool for assessing the 3D orientation of the microstructures in biological tissues such as axons and fibers. DTI measures the self-diffusion of the water molecules in the tissue. In tissue with an isotropic microstructure, the measured diffusion constant is identical in every 3D direction, in which case the diffusion is referred to as isotropic (Basser and Pierpaoli, 1996). In directionally organized tissues, such as brain white matter or muscle, the structural organization of the tissue introduces directional anisotropy in the diffusion process, in which case the diffusion is referred to as anisotropic. Thus, a DTI measurement of the diffusion anisotropy provides information on the underlying tissue architecture. DTI has been frequently used in neural network imaging in brain (Mori and Zhang, 2006; Mori et al., 2007; Mukherjee et al., 2008) and fiber imaging in heart (Buckberg et al., 2006; Strijkers et al., 2009), skeletal muscle (Heemskerk et al., 2009; Lansdown et al., 2007) and cartilage (Filidoro et al., 2005; Pierce et al., 2010). The technique has recently been applied for fiber imaging in healthy arteries (Ghazanfari et al., 2012; Flamini et al., 2015, 2010, 2013).

The current study aimed to assess the 3D fiber orientation and architecture in atherosclerotic carotid plaques with a state-of-the-art DTI technique. Ultimately, this knowledge will provide the essential information for accurate mechanical characterization of carotid plaques in biomechanical models for plaque rupture risk assessment.

2. Materials and methods

2.1. Carotid plaque samples and DTI measurements

Carotid endarterectomy specimens from seven patients (all male, age 55–80 years), with a stenosis > 70%, were imaged in the study. The study protocol was approved by the Medical Ethics Committee of the Erasmus Medical Center and conformed to the ethical guidelines of the 1975 Declaration of Helsinki. This included written informed consents from the patients. Following the endarterectomy, the plaque samples were snap-frozen and stored in a freezer at −80 °C until the day of the DTI measurements. Before imaging, the samples were thawed at room temperature and embedded in 4% agarose type VII in a cryovial, following a protocol described previously in detail (Ghazanfari et al., 2012), to prevent tissue degradation due to contact with air.

DTI was performed with a 9.4 T horizontal bore MRI scanner (Bruker, Ettlingen, Germany) using a dedicated 35-mm diameter send-receive quadrature birdcage radiofrequency coil. A 3D spin-echo DTI sequence with uni-polar diffusion sensitizing pulsed field gradients, placed symmetrically around the 180° radiofrequency pulse, was used. Sequence parameters were as follows: echo time = 27 ms, repetition time = 1000 ms, number of averages = 1, field of view = between 30 × 30 × 30 mm^3 and 30 × 30 × 60 mm^3, depending on the carotid specimen length, acquisition matrix = 96 × 96 × 256, reconstruction matrix = 256 × 256 × 256, 10 diffusion directions with diffusion weighting b-value = 1500 s/mm^2, 1 image without diffusion weighting (b-value = 0).

The careful choice of the settings mentioned above are based on the reasoning as follows: In DTI, the self-diffusion (Brownian motion) of water molecules are probed in a typical timescale of ~10 ms which translates into a diffusion distance of < 5 μm, that is much smaller than the average DTI voxel dimension (in the order of 100 μm). This ensures that the measured apparent diffusion constant and its directional anisotropy are independent on the voxel size and shape, provided the fiber orientation within a voxel is roughly uniform. Moreover, application of diffusion gradients in 10 directions, uniformly distributed over a sphere and independent of voxel shape, prevents a directional bias. Although only 6 orthogonal diffusion-weighted acquisitions (+1 non-weighted image) is sufficient for estimation of the diffusion tensor, to prevent bias in fiber-orientation estimates it is better to use more gradient directions according to an optimized scheme (using a repulsive forces algorithm). However, the error in diffusion estimates is essentially independent on the number of diffusion directions for number of directions larger than 10 (Froeling et al., 2013). Typical apparent diffusion constant in fibrotic tissue at room temperature is in the range of 0.0008–0.0012 mm^2/s. Hence, the chosen b-value of 1500 s/mm^2 ensured that the signal intensities in the diffusion weighted images are in the order of 20–30% of the unweighted images. This provides a signal-to-noise ratio for the diffusion weighted images that are still sufficiently high to prevent a noise bias, and at the same time a sufficiently attenuated signal revealing the diffusion anisotropy. The chosen time of repetition (TR) is a compromise to limit the total acquisition time. It was previously shown that TR = 1000 ms provides sufficient accuracy in cardiovascular tissue (Ghazanfari et al., 2015). In the end, the total acquisition time per sample was approximately 28 h. Furthermore, for DTI one should strive for isotropic or close-to-isotropic voxel dimensions to prevent differential averaging of fiber orientations (Oouchi et al., 2007). In this study, DTI acquisitions were performed with the above-mentioned field of view size and matrix size to achieve close-to-isotropic voxels, and based on previous work (Ghazanfari et al., 2012; Savadjiev et al., 2012; Strijkers et al., 2009), the anisotropy is anticipated to have a negligible effect on the current DTI measurements.

2.2. Assessment of fiber directions and architecture

For qualitative assessment of the fiber orientation and architecture, fiber tractography was performed on the DTI data first, using the open source DTI data visualization tool vIST/e (Vilanova et al., 2006). For quantitative assessment, the raw DTI data was transferred into the MATLAB environment (version 8.1, The MathWorks Inc., Natick, MA) via in-house developed MATLAB scripts. The obtained MRI data did not only contain DTI data (more specifically diffusion tensors, one per voxel) but also T2-weighted images of the plaque from the acquisition with b-value = 0. The lumen and the outer plaque border contours were drawn on the transversal T2-weighted images of the plaques to delineate the plaque area and create a mask for the rest. To downsample the acquired DTI data to a data set with sufficiently detailed information, every 8th transversal image in the longitudinal plaque direction was selected for further analyses. Depending on the length of the plaque sample, the selection resulted in 10 to 18 cross-sections per plaque and 85 cross-sections in total. For each voxel from the plaque tissue, the first eigenvector of the diffusion tensor from the voxel was calculated and used as the measure for the predominant fiber direction in the plaque material in the voxel. The predominant fiber direction data was later transformed from the 3D global Cartesian coordinate system into the local cylindrical system to determine the radial, circumferential and longitudinal components (Fig. 1).

The elevation and azimuthal angles of the predominant fiber directions were calculated (Fig. 1). The elevation angle was defined as the

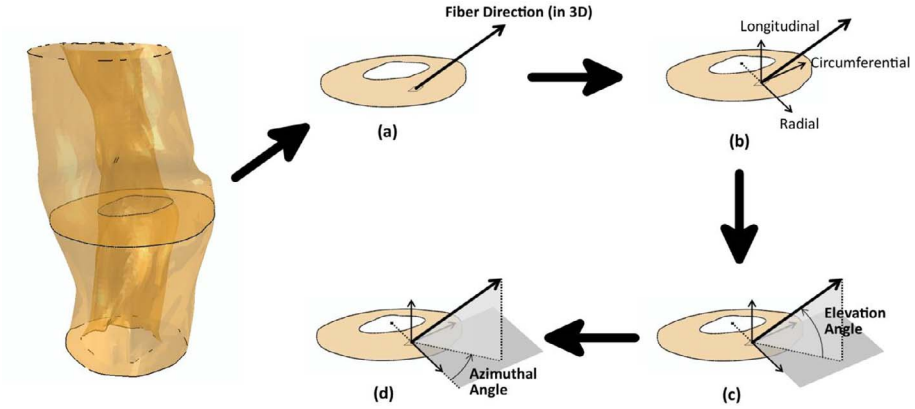

Fig. 1. Cylindrical coordinate system, and the elevation and azimuthal angles were used for the quantitative analysis of the DTI data for the predominant fiber orientations.

angle between the fiber direction and the transversal cross-sectional plane (range = [0–90°], 0° = on the transversal plane and 90° = in the longitudinal direction of the vessel). The azimuthal angle was defined as the angle between the projection of the fiber direction on the transversal plane and the radial direction of the local cylindrical coordinate system (range = [0–360°], 0° & 180° = radial direction, 90° & 270° = circumferential direction). A quantitative analysis was performed to identify to which principal cylindrical direction (radial, circumferential or longitudinal) each predominant fiber orientation was closest. An elevation angle larger than 45° presented a principal longitudinal orientation. In case of an elevation angle smaller than 45°, the principal orientation was defined as circumferential if the azimuthal angle was between 45° and 135°, and as radial otherwise. For further quantitative analysis, the relative amount of the predominant fiber directions was assessed with respect to the elevation and azimuthal angles. The data was analyzed for geometrically concentric and eccentric cross-sections separately. A cross-section was classified as concentric if the eccentricity index, defined as the ratio of the maximum to the minimum plaque thickness in the cross-section, was smaller than 1.5 and as eccentric if otherwise (Li et al., 2010; Ohara et al., 2008).

3. Results

3.1. Fiber architecture in a representative plaque sample

A color-coded tractography image of one of the plaques is shown in the left panel of Fig. 2 (min length of fiber tracked = 5 mm, max fiber angle per step = 45°, seed distance = 1 mm). The fibrillar structures in the image represent the predominant fiber directions and each one of the red, blue and green colors represents an axis-direction (x-,y-, or z-direction) of the 3D Cartesian coordinate system. The dominance of the green color in the image illustrates that the predominant fiber orientations in the region viewed were majorly closest to the longitudinal direction. The right panel in Fig. 2 (middle panel) demonstrates the principal orientation of the predominant fiber directions in four selected cross-sections from the plaque. The longitudinal and circumferential principal orientations prevail in the cross-sections whereas the radial orientation is minimal. The elevation and azimuthal angle histograms (Fig. 2, right panel) demonstrate the variance in fiber orientation among cross-sections.

In total, 11 transversal cross-sections (four concentric and seven eccentric) were obtained from this plaque. The quantitative analysis on these cross-sections demonstrated that, on average, 48% of the predominant fiber orientations were closest to the circumferential direction, 45% to the longitudinal direction and the rest (6%) to the radial direction. The predominant fiber orientations in eccentric cross-sections had mainly elevation angles lower than 60° (Fig. 3, upper panel, left). The concentric cross-sections showed an elevation angle distribution with two discernable peaks: one at 0° and another one around 70° (Fig. 3, upper panel, right). For the azimuthal angle, both eccentric and concentric cross-sections had similar distributions, with two peaks, one around 90° and another one around 270° (Fig. 3, lower panel), indicating that the transversal-plane component of the fibers was majorly in the circumferential direction.

3.2. The general picture of the fiber architecture in carotid plaques

3D fiber orientations in 85 transversal cross-sections from the seven carotid plaques were analyzed to assess the fiber architecture in the carotid plaques. Twenty-three cross-sections were geometrically

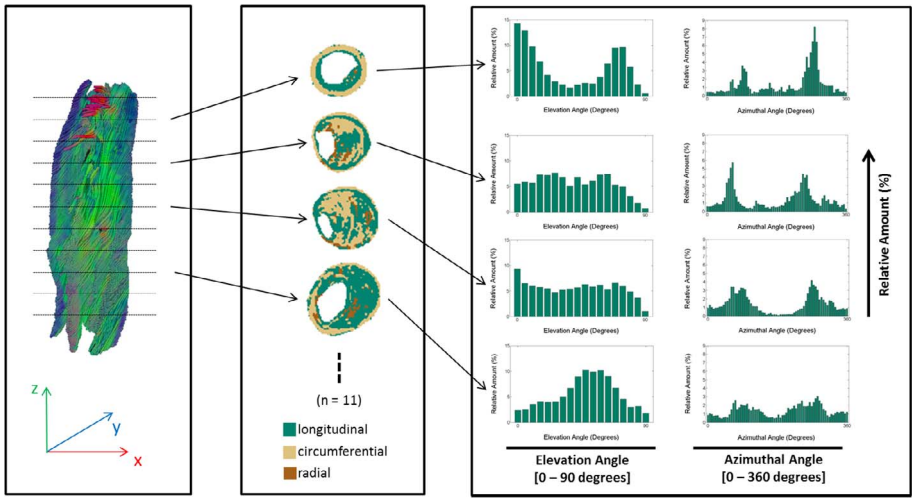

Fig. 2. Color-coded tractography image of a carotid plaque sample (left panel) and principal predominant fiber orientations in four selected transversal cross-sections (mid panel), together with elevation and azimuthal angle histograms (right panel). The setting used for the illustrative tractography image is as follows: min length of fiber tracked = 5 mm, max fiber angle per step = 45 °, seed distance = 1 mm. The bin size in the histograms is 5°.

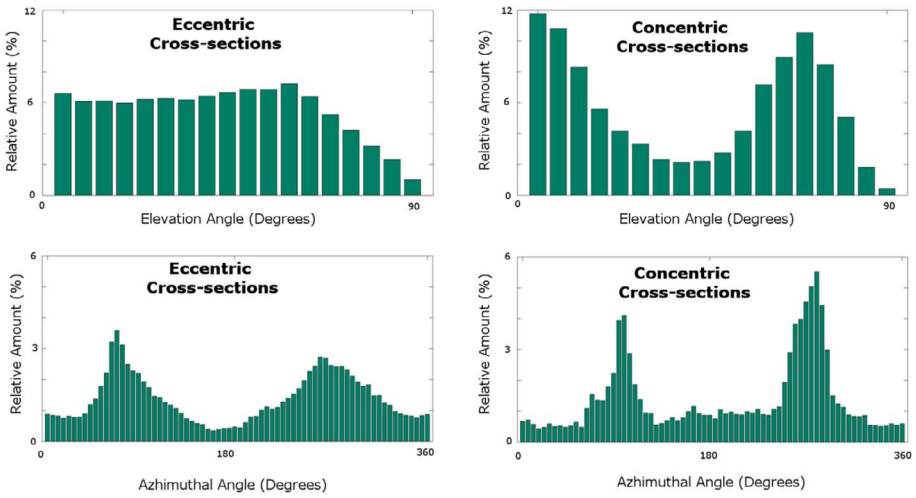

Fig. 3. Relative distribution of the elevation angle (upper panel) and azimuthal angle (lower panel) of the predominant fiber orientations in eccentric (n = 7, left) and concentric cross-sections (n = 4, right) of a carotid plaque sample. The bin size in the histograms is 5°.

concentric and the others (n = 62) were eccentric. The median cross-sectional plaque area was 41 mm^2, where the concentric cross-sections showed statistically significantly smaller plaque area than the eccentric ones (median plaque area of 29.2 mm^2 vs. 48.5 mm^2, $p < 0.001$ in Wilcoxon rank sum test).

All 85 cross-sections combined, 52% of the predominant fiber orientations were closest to the circumferential direction (standard deviation (SD) = 4%), 34% to the longitudinal direction (SD = 7%), and 14% to the radial direction (SD = 5%), on average per plaque. The presence of such large amount of fibers with predominant longitudinal orientation was confirmed by further evidence collected from histology performed on a longitudinal slice of one the tested carotid plaque samples (Fig. 4). Histology was performed by using Resorcin Fuchsin stain for fiber visualization. With this stain elastin fibers are dyed in dark purple, collagen fibers in red pink and the cytoplasm in yellow. Visual inspection of the acquired histology image confirmed the presence of longitudinally aligned collagen fibers. For an objective confirmation, fiber orientations in a subregion on the slice (zoom-in area in Fig. 4) were evaluated by using image processing tools available in MATLAB ("Canny edge detection" and "Watershed" algorithms as described previously (Douglas et al., 2017)). Fibers in this juxtaluminal plaque area showed a predominant longitudinal orientation, demonstrated by the histogram in the lower panel of the figure, where an angle of 90° corresponds to the longitudinal direction. Here, it should be noted that histology is restricted to the cutting plane of the cross-section and cannot provide structural information in the third, out-of-plane dimension. Hence, a longitudial histology slice provides information about the longitudinal and radial components of fiber directions only.

There was no statistically significant difference in the relative

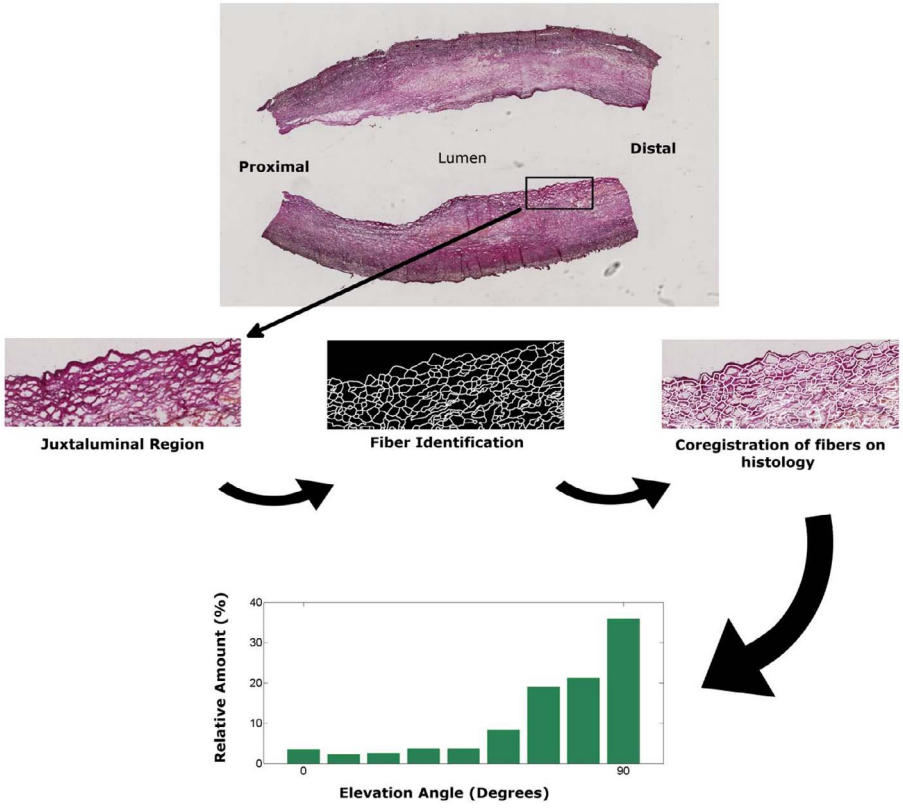

Fig. 4. Histology image of a longitudinal plaque cross-section, stained with Resorcin Fuchsin for visualizing fibers (top panel). Elastin fibers have dark purple color, collagen fibers red pink and the cytoplasm is yellow. The predominant longitudinal orientation of the fibers in some regions, such as the close-up region (middle panel), is discernable. For illustrative purposes, the fibers of this juxtaluminal region were identified from the histology image, using "Canny edge detection" and "Watershed" algorithms in MATLAB (version 8.1) as previously described (Douglas et al., 2017). The majority of the fibers were quantified to have a predominant longitudinal orientation (bar graph in the lower panel, 0° = radial and 90° = longitudinal).

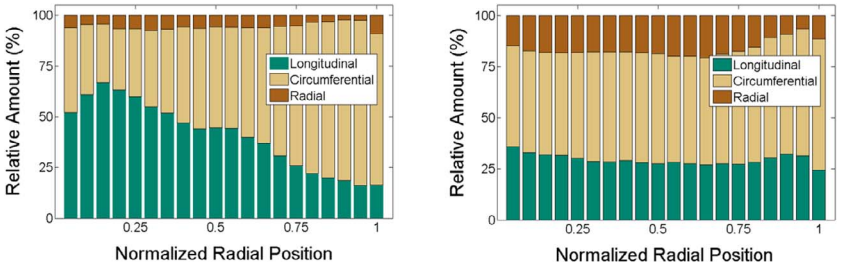

Fig. 5. Relative amount of three principal fiber orientations (longitudinal, circumferential and radial) with respect to radial position in concentric (left panel) and eccentric plaque cross-sections (right panel).

amount of the principal fiber alignments between the concentric and eccentric plaque areas. However, visual inspection and quantitative analysis demonstrated a clear difference with respect to the location. For a visual illustration, the reader is referred to the difference between the fiber alignments in the concentric cross-section (top cross-section) and the eccentric ones (the other three cross-sections) in the middle panel of Fig. 2. In concentric cross-sections, the predominant fiber orientations with a principal alignment in the longitudinal direction were located more juxtaluminally (median relative radius = 0.43, with the relative radius ranging from 0 [lumen] to 1 [outer plaque border] by definition), compared to the ones with principal alignment in the circumferential direction (median relative radius = 0.56). The non-parametric Wilcoxon rank sum test showed that the difference was statistically significant ($p < 0.001$). The relative amount of the fibers with principal longitudinal alignment was up to 70% in the juxtaluminal regions (Fig. 5, left panel) and gradually reduced to ~20% in the outward radial direction, where the balance tipped off towards principal circumferential orientation. Eccentric cross-sections did not show a distinctive structural organization of longitudinally and circumferentially oriented fibers (median relative radius = 0.48 vs 0.49). In eccentric plaques the amount of the principal fiber orientations (longitudinal, circumferential and radial) did not depend on the radial position (Fig. 5, right panel).

Fig. 6 demonstrates the elevation and azimuthal angle distributions combined to depict the predominant fiber directions in 3D for eccentric (upper panel) and concentric cross-sections (lower panel). The histograms for the elevation angle only and for azimuthal angle only are also provided in the graphs. Irrespective of the shape of the cross-sections (eccentric or concentric), two peaks in the 3D distribution maps were discernable: one at an azimuthal angle of 90° and another one at 270°, both with an elevation angle of 0°. This indicated that most fibers had mainly circumferential orientation with a small elevation from the transversal plane. These peaks were higher for the concentric cross-sections.

The histogram of the azimuthal angle for the eccentric cross-sections (Fig. 6, upper panel, azimuthal angle-only histogram) illustrates that 33% of the predominant fiber orientations had an azimuthal angle between 45° and 135° and 40% had an angle between 225° and 315°. For concentric cross-sections (Fig. 6, lower panel, azimuthal angle-only histogram), the values were 35% and 46%, respectively. Moreover, in the concentric cross-sections the peaks in the azimuthal angle distribution were higher. The total relative amount of the predominant fiber orientations with the azimuthal angles 90° ± 22.5° and 270° ± 22.5° was 57% for the concentric cross-sections, whereas the value was 45% for the eccentric ones.

The histogram for the elevation angle in the eccentric cross-sections (Fig. 6, upper panel, elevation angle-only histogram) confirmed the results of the 3D distribution map of the elevation and azimuthal angles combined: the majority of the predominant fiber orientations was on the transversal plane or close to it, indicated by small elevation angles. Sixty-nine percent of the predominant fiber orientations had an elevation angle of smaller than 45° and for 31% of the orientations the angle was greater than 45°. For concentric cross-sections (Fig. 6, lower panel, elevation angle-only histogram), the percentage amounts were comparable to the eccentric cross-sections (66% vs 34%); yet, the distribution showed a different pattern where two peaks in the elevation angle, one at 0° and another one around 65°, were clearly discernable.

4. Discussion

The quantitative analysis of DTI data from the seven endarterectomy samples demonstrated that the predominant 3D fiber orientation in approximately half of the volume in advanced stage carotid plaques is in the circumferential direction with zero or close to zero elevation angles. The main in vivo mechanical loading exerted on arteries in vivo is due to the cyclic blood pressure and is in the circumferential direction. The predominant circumferential alignment of the fibers in healthy arteries and its significant role in arterial load bearing capacity have been demonstrated previously (Cardiovascular Solid Mechanics – Cells, Tissues, and Organs|Jay D. Humphrey|Springer, n.d.; Holzapfel, 2008; Holzapfel et al., 2002; Sáez et al., 2016). As plaques are structurally integral parts of the vasculature at the lesion sites, the circumferential fiber orientation in plaques is likely to contribute to the overall load carrying capacity of the artery and provide mechanical stability to the plaque in this primary in vivo loading direction.

This study also demonstrated the presence of a substantial amount (~1/3 of the plaque volume) of predominant fiber orientations closest to the longitudinal direction. Although a few studies (Orekhov et al., 1987; Pagiatakis et al., 2015) provided observational evidence for longitudinal fiber alignment in atherosclerotic plaques before, this important plaque characteristic is usually overlooked as the traditional way of examining plaque structures are done via histology performed on transversal plaque cross-sections.

For concentric cross-sections, the longitudinal fiber orientation was majorly located in the juxtaluminal regions, revealed by both visual inspection and the statistical analysis, whereas no such structural organization was discernable in the eccentric cross-sections. This difference might be due to the different progression stages of the lesions in the two geometric cross-section types. The concentric cross-sections displayed relatively less advanced phenotype. Longitudinally oriented fibers and SMCs in the juxtaluminal regions of healthy arteries have been previously reported (Canham et al., 1989; Clark and Glagov, 1985; Orekhov et al., 1987; Stehbens, 1960; Timmins et al., 2010). It is likely, that at the onset of an atherosclerotic lesion the longitudinally oriented SMCs in the juxtaluminal regions produce collagen fibers in this direction, whereas the SMCs located deeper in the plaque tissue, possibly transmigrated from the tunica media, produce fibers in the circumferential direction. As the plaque further progresses into a more advanced phenotype, due to the various biological processes involved, the organization of the fiber alignments becomes less structured.

It is also remarkable that in a previous experimental study (Holzapfel et al., 2005), the optimal average fiber elevation angle was calculated to be 60° for “nonatherosclerotic intimal thickening” regions in human coronary arteries as this provided the best fit to the mechanical testing results. This reported value is in accordance with our finding of a large group of fibers with higher elevation angle (~65°) in the concentric cross-sections, which are possibly comparable to the

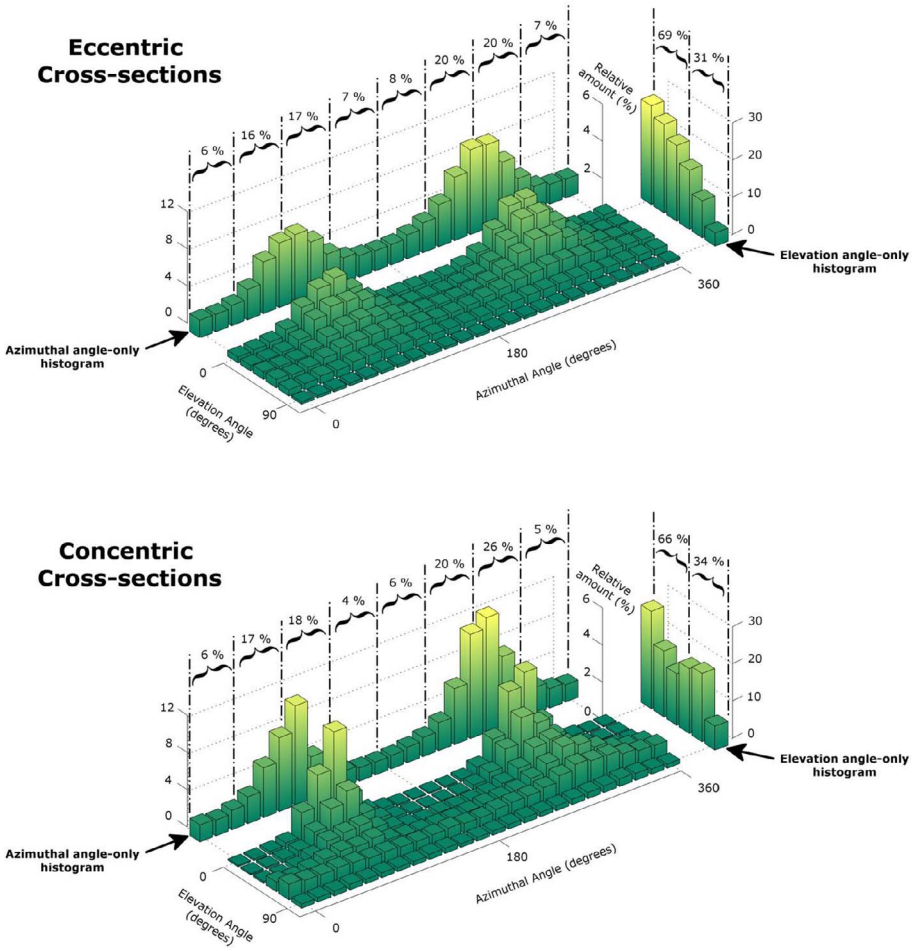

Fig. 6. The combined relative distribution maps of the elevation and azimuthal angles of the predominant fiber orientations in all eccentric (n = 62, upper panel) and all concentric cross-sections (n = 23, lower panel) from the seven plaque samples imaged. (The bin size is 15° × 15°.) The histograms of the elevation angle only and azimuthal angle only are also provided in the graphs.

"nonatherosclerotic intimal thickening" regions tested in the above-mentioned study.

The current study has a number of limitations, some of which are inherent to the imaging technique used. DTI is a powerful method to assess the fiber organization in biological tissues. However, it does not directly image individual fibers. Therefore, it was not possible to determine the amount, the density or the type of the fibers in the plaques. A further analysis was performed by segmenting out dark regions visible on the T2-weighted images, which are most likely calcified regions (Shinnar et al., 1999), with minimal fiber content. The volume of the segmented dark regions was 10% of the total plaque volume and excluding the regions had almost no effect (< 4%) on the fiber orientation results. It has also to be noted that the plaques were imaged under load-free conditions. The carotid arteries are subjected to longitudinal pre-stretch in situ (Horný et al., 2016), hence slightly higher elevation angles for the plaque fibers are to be expected in vivo. It is also possible that (some) collected endarterectomy specimens contained a certain amount of medial layer as the outer border since dissection plane in the procedure might have deviated from the intended internal elastic lamina as reported before (Roberts et al., 2007). This might have introduced a slight bias in the results towards a greater relative amount measurement in the circumferential orientation.

The fiber orientation in biological tissues is a major determinant of tissue mechanical behavior. Its importance for mechanical stresses and stability of atherosclerotic plaques has also been demonstrated previously in a numerical study (Liang et al., 2013). However, the biomechanical models of atherosclerotic plaques developed so far did not incorporate 3D plaque fiber orientations due to the unavailability of this fundamental information. This study provides this missing knowledge for carotid plaques and to the best of the authors' knowledge, is the first to assess the 3D fiber orientation in atherosclerotic plaques in general. The acquired unique information on 3D plaque fiber direction will pave the road to more realistic biomechanical plaque modeling for stress analyses and mechanical stability assessment.

Conflict of interest

None.

Financial support

This work was supported by the "Stichting voor de Technische Wetenschappen" [OTP-12548].

References

Akyildiz, A.C., Speelman, L., van Brummelen, H., Gutiérrez, M.A., Virmani, R., van der Lugt, A., van der Steen, A.F., Wentzel, J.J., Gijsen, F.J., 2011. Effects of intima stiffness and plaque morphology on peak cap stress. Biomed. Eng. OnLine 10, 25. http://dx.doi.org/10.1186/1475-925X-10-25.

Akyildiz, A.C., Speelman, L., Nieuwstadt, H.A., van Brummelen, H., Virmani, R., van der Lugt, A., van der Steen, A.F.W., Wentzel, J.J., Gijsen, F.J.H., 2015. The effects of plaque morphology and material properties on peak cap stress in human coronary arteries. Comput. Methods Biomech. Biomed. Eng. 1–9. http://dx.doi.org/10.1080/10255842.2015.1062091.

Barnes, M.J., Farndale, R.W., 1999. Collagens and atherosclerosis. Exp. Gerontol. 34, 513–525.

Bartoš, F., Ledvina, M., 1979. Collagen, elastin and desmosines in three layers of bovine aortas of different ages. Exp. Gerontol. 14, 21–26. http://dx.doi.org/10.1016/0531-5565(79)90004-4.

Basser, P.J., Pierpaoli, C., 1996. Microstructural and physiological features of tissues elucidated by quantitative-diffusion-tensor MRI. J. Magn. Reson. B 111, 209–219.

Buckberg, G.D., Mahajan, A., Jung, B., Markl, M., Hennig, J., Ballester-Rodes, M., 2006. MRI myocardial motion and fiber tracking: a confirmation of knowledge from

different imaging modalities. Eur. J. Cardio-Thorac. Surg. 29 (Suppl 1), S165–177. http://dx.doi.org/10.1016/j.ejcts.2006.02.064.

Canham, P.B., Finlay, H.M., Dixon, J.G., Boughner, D.R., Chen, A., 1989. Measurements from light and polarised light microscopy of human coronary arteries fixed at distending pressure. Cardiovasc. Res. 23, 973–982.

Cardiovascular Solid Mechanics – Cells, Tissues, and Organs | Jay D. Humphrey | Springer, n.d.

Carr, S., Farb, A., Pearce, W.H., Virmani, R., Yao, J.S., 1996. Atherosclerotic plaque rupture in symptomatic carotid artery stenosis. J. Vasc. Surg. 23, 755–765 discussion 765–766.

Chai, C.-K., Akyildiz, A.C., Speelman, L., Gijsen, F.J.H., Oomens, C.W.J., van Sambeek, M.R.H.M., van der Lugt, A., Baaijens, F.P.T., 2015. Local anisotropic mechanical properties of human carotid atherosclerotic plaques – characterisation by micro-indentation and inverse finite element analysis. J. Mech. Behav. Biomed. Mater. 43, 59–68. http://dx.doi.org/10.1016/j.jmbbm.2014.12.004.

Chen, H., Kassab, G.S., 2016. Microstructure-based biomechanics of coronary arteries in health and disease. J. Biomech. 49, 2548–2559. http://dx.doi.org/10.1016/j.jbiomech.2016.03.023.

Cheng, G.C., Loree, H.M., Kamm, R.D., Fishbein, M.C., Lee, R.T., 1993. Distribution of circumferential stress in ruptured and stable atherosclerotic lesions. A structural analysis with histopathological correlation. Circulation 87, 1179–1187. http://dx.doi.org/10.1161/01.CIR.87.4.1179.

Clark, J.M., Glagov, S., 1985. Transmural organization of the arterial media. The lamellar unit revisited. Arterioscler. Dallas Tex 5, 19–34.

Deguchi, J.-O., Aikawa, E., Libby, P., Vachon, J.R., Inada, M., Krane, S.M., Whittaker, P., Aikawa, M., 2005. Matrix metalloproteinase-13/collagenase-3 deletion promotes collagen accumulation and organization in mouse atherosclerotic plaques. Circulation 112, 2708–2715. http://dx.doi.org/10.1161/CIRCULATIONAHA.105.562041.

Douglas, G.R., Brown, A.J., Gillard, J.H., Bennett, M.R., Sutcliffe, M.P.F., Teng, Z., 2017. Impact of fiber structure on the material stability and rupture mechanisms of coronary atherosclerotic plaques. Ann. Biomed. Eng. 1–13. http://dx.doi.org/10.1007/s10439-017-1827-3.

Filidoro, L., Dietrich, O., Weber, J., Rauch, E., Oerther, T., Wick, M., Reiser, M.F., Glaser, C., 2005. High-resolution diffusion tensor imaging of human patellar cartilage: feasibility and preliminary findings. Magn. Reson. Med. 53, 993–998. http://dx.doi.org/10.1002/mrm.20469.

Finlay, H.M., McCullough, L., Canham, P.B., 1995. Three-dimensional collagen organization of human brain arteries at different transmural pressures. J. Vasc. Res. 32, 301–312.

Flamini, V., Creane, A.P., Kerskens, C.M., Lally, C., 2015. Imaging and finite element analysis: a methodology for non-invasive characterization of aortic tissue. Med. Eng. Phys. 37, 48–54. http://dx.doi.org/10.1016/j.medengphy.2014.10.006.

Flamini, V., Kerskens, C., Moerman, K.M., Simms, C.K., Lally, C., 2010. Imaging arterial fibres using diffusion tensor imaging—feasibility study and preliminary results. EURASIP J. Adv. Signal Process. 2010, 904091. http://dx.doi.org/10.1155/2010/904091.

Flamini, V., Kerskens, C., Simms, C., Lally, C., 2013. Fibre orientation of fresh and frozen porcine aorta determined non-invasively using diffusion tensor imaging. Med. Eng. Phys. 35, 765–776. http://dx.doi.org/10.1016/j.medengphy.2012.08.008.

Fratzl, P., 2008. Collagen: Structure and Mechanics. Springer Science & Business Media.

Froeling, M., Nederveen, A.J., Nicolay, K., Strijkers, G.J., 2013. DTI of human skeletal muscle: the effects of diffusion encoding parameters, signal-to-noise ratio and T2 on tensor indices and fiber tracts. NMR Biomed. 26, 1339–1352. http://dx.doi.org/10.1002/nbm.2959.

Ghazanfari, S., Driessen-Mol, A., Strijkers, G.J., Baaijens, F.P.T., Bouten, C.V.C., 2015. The evolution of collagen fiber orientation in engineered cardiovascular tissues visualized by diffusion tensor imaging. PLOS ONE 10, e0127847. http://dx.doi.org/10.1371/journal.pone.0127847.

Ghazanfari, S., Driessen-Mol, A., Strijkers, G.J., Kanters, F.M.W., Baaijens, F.P.T., Bouten, C.V.C., 2012. A comparative analysis of the collagen architecture in the carotid artery: second harmonic generation versus diffusion tensor imaging. Biochem. Biophys. Res. Commun. 426, 54–58. http://dx.doi.org/10.1016/j.bbrc.2012.08.031.

Heemskerk, A.M., Sinha, T.K., Wilson, K.J., Ding, Z., Damon, B.M., 2009. Quantitative assessment of DTI-based muscle fiber tracking and optimal tracking parameters. Magn. Reson. Med. 61, 467–472. http://dx.doi.org/10.1002/mrm.21819.

Holzapfel, G.A., 2008. Collagen in Arterial Walls: Biomechanical Aspects. In: Fratzl, P. (Ed.), Collagen. Springer US, pp. 285–324. doi: 10.1007/978-0-387-73906-9_11.

Holzapfel, G.A., Gasser, T.C., Stadler, M., 2002. A structural model for the viscoelastic behavior of arterial walls: continuum formulation and finite element analysis. Eur. J. Mech. – A Solids 21, 441–463. http://dx.doi.org/10.1016/S0997-7538(01)01206-2.

Holzapfel, G.A., Sommer, G., Gasser, C.T., Regitnig, P., 2005. Determination of layer-specific mechanical properties of human coronary arteries with nonatherosclerotic intimal thickening and related constitutive modeling. Am. J. Physiol. Heart Circ. Physiol. 289, H2048–2058. http://dx.doi.org/10.1152/ajpheart.00934.2004.

Horný, L., Adámek, T., Kulvajtová, M., 2016. A comparison of age-related changes in axial prestretch in human carotid arteries and in human abdominal aorta. Model. Mechanobiol. Biomech. http://dx.doi.org/10.1007/s10237-016-0797-y.

Hosoda, Y., Kawano, K., Yamasawa, F., Ishii, T., Shibata, T., Inayama, S., 1984. Age-dependent changes of collagen and elastin content in human aorta and pulmonary artery. Angiology 35, 615–621.

Humphrey, J.D., 2002. Cardiovascular Solid Mechanics: Cells, Tissues, and Organs. Springer Science & Business Media.

Lansdown, D.A., Ding, Z., Wadington, M., Hornberger, J.L., Damon, B.M., 2007. Quantitative diffusion tensor MRI-based fiber tracking of human skeletal muscle. J. Appl. Physiol. Bethesda Md 1985 (103), 673–681. http://dx.doi.org/10.1152/japplphysiol.00290.2007.

Li, F., McDermott, M.M., Li, D., Carroll, T.J., Hippe, D.S., Kramer, C.M., Fan, Z., Zhao, X., Hatsukami, T.S., Chu, B., Wang, J., Yuan, C., 2010. The association of lesion eccentricity with plaque morphology and components in the superficial femoral artery: a high-spatial-resolution, multi-contrast weighted CMR study. J. Cardiovasc. Magn. Reson. Off. J. Soc. Cardiovasc. Magn. Reson. 12, 37. http://dx.doi.org/10.1186/1532-429X-12-37.

Liang, X., Xenos, M., Alemu, Y., Rambhia, S.H., Lavi, I., Kornowski, R., Gruberg, L., Fuchs, S., Einav, S., Bluestein, D., 2013. Biomechanical factors in coronary vulnerable plaque risk of rupture: intravascular ultrasound-based patient-specific fluid-structure interaction studies. Coron. Artery Dis. 24, 75–87. http://dx.doi.org/10.1097/MCA.0b013e32835bbe99.

Mayne, R., 1986. Collagenous proteins of blood vessels. Arterioscler. Dallas Tex 6, 585–593.

Mori, S., Zhang, J., 2006. Principles of diffusion tensor imaging and its applications to basic neuroscience research. Neuron 51, 527–539. http://dx.doi.org/10.1016/j.neuron.2006.08.012.

Mori, T., Ohnishi, T., Hashimoto, R., Nemoto, K., Moriguchi, Y., Noguchi, H., Nakabayashi, T., Hori, H., Harada, S., Saitoh, O., Matsuda, H., Kunugi, H., 2007. Progressive changes of white matter integrity in schizophrenia revealed by diffusion tensor imaging. Psychiatry Res. 154, 133–145. http://dx.doi.org/10.1016/j.pscychresns.2006.09.004.

Mukherjee, P., Berman, J.I., Chung, S.W., Hess, C.P., Henry, R.G., 2008. Diffusion tensor MR imaging and fiber tractography: theoretic underpinnings. AJNR Am. J. Neuroradiol. 29, 632–641. http://dx.doi.org/10.3174/ajnr.A1051.

Murata, K., Motayama, T., Kotake, C., 1986. Collagen types in various layers of the human aorta and their changes with the atherosclerotic process. Atherosclerosis 60, 251–262.

Nadkarni, S.K., Pierce, M.C., Park, B.H., de Boer, J.F., Whittaker, P., Bouma, B.E., Bressner, J.E., Halpern, E., Houser, S.L., Tearney, G.J., 2007. Measurement of collagen and smooth muscle cell content in atherosclerotic plaques using polarization-sensitive optical coherence tomography. J. Am. Coll. Cardiol. 49, 1474–1481. http://dx.doi.org/10.1016/j.jacc.2006.11.040.

Newby, A.C., Zaltsman, A.B., 1999. Fibrous cap formation or destruction–the critical importance of vascular smooth muscle cell proliferation, migration and matrix formation. Cardiovasc. Res. 41, 345–360.

Nieuwstadt, H.A., Akyildiz, A.C., Speelman, L., Virmani, R., van der Lugt, A., van der Steen, A.F.W., Wentzel, J.J., Gijsen, F.J.H., 2013. The influence of axial image resolution on atherosclerotic plaque stress computations. J. Biomech. 46, 689–695. http://dx.doi.org/10.1016/j.jbiomech.2012.11.042.

Ohara, T., Toyoda, K., Otsubo, R., Nagatsuka, K., Kubota, Y., Yasaka, M., Naritomi, H., Minematsu, K., 2008. Eccentric stenosis of the carotid artery associated with ipsilateral cerebrovascular events. AJNR Am. J. Neuroradiol. 29, 1200–1203. http://dx.doi.org/10.3174/ajnr.A0997.

Oouchi, H., Yamada, K., Sakai, K., Kizu, O., Kubota, T., Ito, H., Nishimura, T., 2007. Diffusion anisotropy measurement of brain white matter is affected by voxel size: underestimation occurs in areas with crossing fibers. Am. J. Neuroradiol. 28, 1102–1106. http://dx.doi.org/10.3174/ajnr.A0488.

Orekhov, A.N., Andreeva, E.R., Tertov, V.V., 1987. The distribution of cells chemical components intima human aorta. In: Chazov, E.I., Smirnov, V.N. (Eds.), Human Atherosclerosis. Harwood Academic Publishers GmbH, pp. 75–93.

Pagiatakis, C., Galaz, R., Tardif, J.-C., Mongrain, R., 2015. A comparison between the principal stress direction and collagen fiber orientation in coronary atherosclerotic plaque fibrous caps. Med. Biol. Eng. Comput. 53, 545–555. http://dx.doi.org/10.1007/s11517-015-1257-z.

Pickering, J.G., Ford, C.M., Chow, L.H., 1996. Evidence for rapid accumulation and persistently disordered architecture of fibrillar collagen in human coronary restenosis lesions. Am. J. Cardiol. 78, 633–637.

Pierce, D.M., Trobin, W., Raya, J.G., Trattnig, S., Bischof, H., Glaser, C., Holzapfel, G.A., 2010. DT-MRI based computation of collagen fiber deformation in human articular cartilage: a feasibility study. Ann. Biomed. Eng. 38, 2447–2463. http://dx.doi.org/10.1007/s10439-010-9990-9.

Reimann, C., Brangsch, J., Colletini, F., Walter, T., Hamm, B., Botnar, R.M., Makowski, M.R., 2016. Molecular imaging of the extracellular matrix in the context of atherosclerosis. Drug Deliv. Rev. Adv. http://dx.doi.org/10.1016/j.addr.2016.09.005.

Rekhter, M.D., Zhang, K., Narayanan, A.S., Phan, S., Schork, M.A., Gordon, D., 1993. Type I collagen gene expression in human atherosclerosis. Localization to specific plaque regions. Am. J. Pathol. 143, 1634–1648.

Richardson, P.D., Davies, M.J., Born, G.V.R., 1989. Influence of Plaque Configuration and Stress Distribution on Fissuring of Coronary Atherosclerotic Plaques. The Lancet, Originally published as Volume 2, Issue 8669 334, 941–944. doi:10.1016/S0140-6736(89)90953-7.

Roberts, W.C., Laborde, N.J., Pearl, G.J., 2007. Frequency and extent of media in the internal carotid artery in “endarterectomy” specimens. Am. J. Cardiol. 99, 990–992. http://dx.doi.org/10.1016/j.amjcard.2006.11.043.

Sáez, P., García, A., Peña, E., Gasser, T.C., Martínez, M.A., 2016. Microstructural quantification of collagen fiber orientations and its integration in constitutive modeling of the porcine carotid artery. Acta Biomater. 33, 183–193. http://dx.doi.org/10.1016/j.actbio.2016.01.030.

Savadjiev, P., Strijkers, G.J., Bakermans, A.J., Piuze, E., Zucker, S.W., Siddiqi, K., 2012. Heart wall myofibers are arranged in minimal surfaces to optimize organ function. Proc. Natl. Acad. Sci. U.S.A. 109, 9248–9253. http://dx.doi.org/10.1073/pnas.1120785109.

Shadwick, R.E., 1999. Mechanical design in arteries. J. Exp. Biol. 202, 3305–3313.

Shekhonin, B.V., Domogatsky, S.P., Muzykantov, V.R., Idelson, G.L., Rukosuev, V.S., 1985. Distribution of type I, III, IV and V collagen in normal and atherosclerotic

human arterial wall: immunomorphological characteristics. Coll. Relat. Res. 5, 355–368.

Shinnar, M., Fallon, J.T., Wehrli, S., Levin, M., Dalmacy, D., Fayad, Z.A., Badimon, J.J., Harrington, M., Harrington, E., Fuster, V., 1999. The diagnostic accuracy of ex vivo MRI for human atherosclerotic plaque characterization. Arterioscler. Thromb. Vasc. Biol. 19, 2756–2761.

Stehbens, W.E., 1960. Focal intimal proliferation in the cerebral arteries. Am. J. Pathol. 36, 289–301.

Strijkers, G.J., Bouts, A., Blankesteijn, W.M., Peeters, T.H.J.M., Vilanova, A., van Prooijen, M.C., Sanders, H.M.H.F., Heijman, E., Nicolay, K., 2009. Diffusion tensor imaging of left ventricular remodeling in response to myocardial infarction in the mouse. NMR Biomed. 22, 182–190. http://dx.doi.org/10.1002/nbm.1299.

Teng, Z., Brown, A.J., Calvert, P.A., Parker, R.A., Obaid, D.R., Huang, Y., Hoole, S.P., West, N.E.J., Gillard, J.H., Bennett, M.R., 2014. Coronary plaque structural stress is associated with plaque composition and subtype and higher in acute coronary syndrome: the BEACON I (Biomechanical Evaluation of Atheromatous Coronary Arteries) study. Circ. Cardiovasc. Imaging 7, 461–470. http://dx.doi.org/10.1161/CIRCIMAGING.113.001526.

Teng, Z., Yuan, J., Feng, J., Zhang, Y., Brown, A.J., Wang, S., Lu, Q., Gillard, J.H., 2015. The influence of constitutive law choice used to characterise atherosclerotic tissue material properties on computing stress values in human carotid plaques. J. Biomech. 48, 3912–3921. http://dx.doi.org/10.1016/j.jbiomech.2015.09.023.

Timmins, L.H., Wu, Q., Yeh, A.T., Moore, J.E., Greenwald, S.E., 2010. Structural inhomogeneity and fiber orientation in the inner arterial media. Am. J. Physiol. Heart Circ. Physiol. 298, H1537–1545. http://dx.doi.org/10.1152/ajpheart.00891.2009.

Vilanova, A., Zhang, S., Kindlmann, G., Laidlaw, D., 2006. An Introduction to Visualization of Diffusion Tensor Imaging and Its Applications, in: Weickert, P.J., Hagen, P.H. (Eds.), Visualization and Processing of Tensor Fields, Mathematics and Visualization. Springer Berlin Heidelberg, pp. 121–153. doi: 10.1007/3-540-31272-2_7.

Walker-Caprioglio, H.M., Trotter, J.A., Mercure, J., Little, S.A., McGuffee, L.J., 1991. Organization of rat mesenteric artery after removal of cells of extracellular matrix components. Cell Tissue Res. 264, 63–77.